Magnetohydrodynamic Turbulent Evolution of a Magnetic Cloud in the Outer Heliosphere

Daniele Telloni[1] , Lingling Zhao[2] , Gary P. Zank[2,3] , Haoming Liang[2] , Masaru Nakanotani[2] , Laxman Adhikari[2] ,
Francesco Carbone[4] , Raffaella D'Amicis[5] , Denise Perrone[6] , Roberto Bruno[5] , and Sergio Dasso[7,8]

[1] National Institute for Astrophysics—Astrophysical Observatory of Torino Via Osservatorio 20, I-10025 Pino Torinese, Italy; daniele.telloni@inaf.it
[2] University of Alabama, Center for Space Plasma and Aeronomic Research, Huntsville, AL 35805, USA
[3] University of Alabama, Department of Space Science, Huntsville, AL 35805, USA
[4] National Research Council—Institute of Atmospheric Pollution Research c/o University of Calabria, I-87036 Rende, Italy
[5] National Institute for Astrophysics—Institute for Space Astrophysics and Planetology Via del Fosso del Cavaliere 100, I-00133 Roma, Italy
[6] Italian Space Agency Via del Politecnico snc, I-00133 Roma, Italy
[7] Universidad de Buenos Aires—Departamento de Ciencias de la Atmósfera y los Océanos, Buenos Aires, C1428EGA, Argentina
[8] Universidad de Buenos Aires—Instituto de Astronomía y Física del Espacio, Buenos Aires, C1428EGA, Argentina
Received 2020 September 29; revised 2020 November 8; accepted 2020 November 17; published 2020 December 11

Abstract

This Letter exploits joint observations of the same interplanetary coronal mass ejection by widely separated spacecraft to study, for the first time, the turbulent evolution of the magnetohydrodynamic (MHD) properties of the embedded magnetic cloud, during its propagation throughout interplanetary space. Specifically, the event was observed by Wind at 1 au on 1998 March 4–6 and tracked to the location of Ulysses at 5.4 au 18 days later, when the two spacecraft were radially aligned with the Sun. The analysis of the MHD invariants within the magnetic cloud, along with its energy budget, provides compelling evidence of magnetic erosion of the structure thanks to its interaction with a trailing magnetic cloud. The helical configuration is thus largely deformed and degraded, and the initial dominance of magnetic over kinetic energy is observed to evolve toward a less imbalanced condition. This is consistent with the expected conversion of magnetic energy into kinetic energy due to magnetic reconnection processes. Local interaction of the magnetic cloud's (MC) outer layers with the solar wind acts to generate larger amplitude Alfvénic fluctuations in the downstream region, leading the MC to turbulently evolve toward a more complex cross-helicity configuration in the outer heliosphere. Finally, evidence of a flux rope locally generated by magnetic reconnection events at 1 au that likely decays by the time it reaches Ulysses is also reported.

Unified Astronomy Thesaurus concepts: Magnetohydrodynamics (1964); Interplanetary turbulence (830); Solar coronal mass ejections (310); Interplanetary magnetic fields (824); Heliosphere (711); Solar wind (1534); Solar magnetic reconnection (1504)

1. Introduction

Interplanetary coronal mass ejections (ICMEs; e.g., Kilpua et al. 2017) are the heliospheric counterparts of large-scale eruptive phenomena occurring at the Sun, in which the free magnetic energy, stored in the complex twisted magnetic field of the solar corona, is released impulsively via magnetic reconnection processes. This triggers the expulsion of coronal material into interplanetary space at such high velocities that they eventually accelerate solar energetic particles (SEPs; Reames 1999). As ICMEs propagate outward, they may strongly interact with the ambient solar wind or with other ICMEs, through a variety of mechanisms, such as magnetic erosion or merging, driven by magnetic reconnection (see the review by Manchester et al. 2017, and references therein). Such interactions can considerably alter the ICME magnetic topology, leading to particularly complex structures.

ICMEs having a flux-rope-like magnetic field configuration are known as magnetic clouds (MCs; Burlaga et al. 1981). Flux ropes (FRs) are solenoid-like magnetic structures consisting of helical field lines wrapped around a cylindrical shape, carrying a strong axial current and an azimuthal magnetic field (Russell & Elphic 1979). Strong observational evidence that the magnetic core of any (I)CME is represented by a flux rope has been provided recently by Vourlidas (2014). Definitive confirmation would require measurements of the 3D magnetic field structure, which is impossible with single-spacecraft observations. It transpires that MCs form just a substructure of the total ICME interval (Gulisano et al. 2010; Richardson & Cane 2010; Lugaz et al. 2020). ICMEs that do not exhibit an MC geometry are thought to have been crossed by the spacecraft at the peripheral regions of the ICME, far from the centrally nested MC. When sampled by a spacecraft, FRs (and, in turn, MCs) are observed in in situ data as large-scale smooth rotations of the magnetic field vector around the radial direction (e.g., Klein & Burlaga 1982; Burlaga 1988; Lepping et al. 1990). Hence, MCs possess considerable magnetic helicity H_m (Moffatt 1978), one of the three invariants of the ideal magnetohydrodynamic (MHD) equations (the others being cross-helicity H_c and total—kinetic plus magnetic—energy E; Matthaeus & Goldstein 1982), which measures the degree of winding of the magnetic field lines. Because of their closed-loop field structure, both sunward and antisunward Alfvénic fluctuations are expected to populate the MC cores, which should be thus characterized by very low cross-helicity (a measure of the energy difference between forward and backward Alfvén modes), as very recently shown by Good et al. (2020). Furthermore, since MCs are magnetic structures, they are characterized by highly negative residual energy E_r (a measure of the imbalance between kinetic and magnetic energies).

An analysis of MHD invariants within MCs allows for their proper identification in the solar wind (Telloni et al. 2019; Zhao et al. 2020a). Furthermore, by exploiting observations of the

same MC gathered at different distances from the Sun by two radially aligned spacecraft, it helps clarify the role played by ideal MHD and magnetic reconnection processes in the turbulent evolution of these structures as they propagate in interplanetary space.

However, instances of ICME encounters by aligned spacecraft are very rare (thus severely compromising the possibility of studying their propagation and evolution). In fact, during the 2006–2015 time period when concurrent space missions were orbiting closer to the Sun (MErcury Surface, Space ENvironment, GEochemistry and Ranging (MESSENGER) and Venus Express) and at 1 au (Wind, Advanced Composition Explorer (ACE), and the twin Solar TErrestrial RElations Observatory (STEREO) satellites), only 45 prominent ICMEs were observed by pairs of spacecraft close to radial alignment (Salman et al. 2020). Alignment of satellites orbiting within and beyond 1 au are even more rare (since the only space mission devoted to solar wind studies and orbiting beyond the Earth, Ulysses, had a polar trajectory and therefore is in the ecliptic plane only for short intervals of time). As one of these few exceptional cases, the ICME observed at 1 au by Wind/ACE and at 5.4 au by Ulysses during a radial alignment in 1998 March has been extensively investigated (Skoug et al. 2000; Du et al. 2007; Nakwacki et al. 2011; Li et al. 2017). Except for Li et al. (2017), where the radial evolution of the embedded Alfvénic fluctuations and their possible role in heating solar wind plasma are studied, these works mainly focus on the kinematical and dynamical evolution of the global morphology (expansion, distortion, deformation, orientation, and propagation direction) experienced by the ICME during its transit from the Sun to the outer heliosphere. These studies almost completely neglect any study of MHD invariants (as magnetic helicity and energy), which are crucial for understanding ICMEs as magnetohydrodynamical structures. Some information about magnetic helicity is provided in Du et al. (2007) and Nakwacki et al. (2011). Unfortunately, these results are not satisfactory, since they depend on the model adopted to retrieve this quantity and on ad hoc assumptions of the (cylindrical) geometry of the flux rope embedded in the ICME that are generally (though not universally; e.g., Al-Haddad et al. 2011) adopted for MCs. A model-independent analysis of the MHD properties (directly measured from in situ spacecraft data) possessed by the ICME and their evolution during propagation is still absent in the literature and motivates the present work.

This Letter observationally explores the MHD turbulent evolution of ICMEs, by exploiting in situ measurements of the same MC observed in 1998 March by two space missions (Wind and Ulysses) radially aligned with the Sun and separated by 4.4 au. A full description of the MHD invariants (magnetic and cross-helicity, and total energy) and the residual energy, computed at both locations, is used to address, for the first time, whether magnetic clouds embedded in ICMEs experience significant changes and/or restructuring or evolve self-similarly during their journey through the solar wind. The role played by the competing mechanisms of magnetic erosion and coalescence in modeling and shaping the MC magnetic field configuration is explored. Specifically, using a robust observational perspective, current hot topics in heliospheric and plasma physics, such as magnetic reconnection phenomena and the conservation or decay of the MHD invariants in space plasma are addressed. The analysis is based on a novel technique advanced by Telloni et al. (2012) (and since then largely

employed in solar wind studies; e.g., Telloni et al. 2013, 2016, 2019; Zhao et al. 2020a, 2020b; Good et al. 2020) for using heliospheric data to identify, in both time and scale, helical structures such as FRs or MCs (i.e., their 2D representation as magnetic helicity events), and to investigate their MHD properties.

The layout of this Letter presents a methodological approach to solar wind data (Section 2), illustrating and discussing the results observed at Wind and Ulysses (Section 3) and concluding remarks (Section 4).

2. Data Analysis

When the MC was observed by Wind (on 1998 March 4 at 12:00 UT) and by Ulysses approximately 18 days later, the two spacecraft lined up near the ecliptic plane with latitudinal and longitudinal separations of just 2° and 5°, respectively. The relative positions of the Wind and Ulysses satellites at the times of the MC encounters are displayed as side (XZ) and top (XY) views of the ecliptic plane in Figure 1 (left and right panel, respectively). A nearly perfect radial alignment occurred between the two spacecraft. This ensures that the same MC plasma is observed first at 1 au by Wind and then at 5.4 au by Ulysses at two different MHD evolution stages.

Combined data sets for the interplanetary magnetic field and solar wind plasma from both Wind and Ulysses spacecraft are analyzed. The Solar Wind Experiment (SWE; Ogilvie et al. 1995) on board Wind and the Solar Wind Observations Over the Poles of the Sun (SWOOPS; Bame et al. 1992) instrument on board Ulysses provide solar wind bulk speed and proton number density measurements. Magnetic field observations come from the Wind/Magnetic Field Investigation (MFI; Lepping et al. 1995) instrument and the Ulysses/Vector Helium Magnetometer (VHM; Balogh et al. 1992). Wind and Ulysses magnetic field measurements are downsampled to comply with the lower-resolution plasma data, to obtain 48 s and 4 minute averaged combined time series, respectively. Wind data are in Geocentric Solar Ecliptic (GSE) coordinates, and Ulysses data are in the heliographic Radial Tangential Normal (RTN) coordinate system. However, no transformation of coordinates from RTN to GSE system is required, since, as shown below, all of the analyzed MHD quantities are invariant under all possible rotational transformations.

The magnetic B and velocity V fields are conveniently separated into mean and fluctuating components, as $B = B_0 + b$ and $V = V_0 + v$, where $B_0 = \langle B \rangle$ is the mean magnetic field with the average fluctuating magnetic field $\langle b \rangle = 0$, and similarly for the velocity field. The Elsässer variables (Elsässer 1950) are expressed as $z^\pm = u \pm \tilde{b}$, where $\tilde{b} = b/\sqrt{4\pi\rho}$ (ρ is the mass density) and the sign in front of $\tilde{b}$ depends on the sign of $-k \cdot B_0$ (k is the wavevector). Hence, $z^\pm$ represent outwardly $(+)$ and inwardly $(-)$ directed Alfvén modes (Bruno & Carbone 2013).

Following the method introduced by Telloni et al. (2012) and generalized by Zhao et al. (2020b), using Paul wavelet transforms $\mathcal{W}$ (Torrence & Compo 1998), and by virtue of Taylor's hypothesis, the magnetic helicity $H_m(t, s)$, cross-helicity $H_c(t, s)$, residual energy $E_r(t, s)$, and total energy $E(t, s)$ can be expressed as functions of time t and scale s, as

$$H_m(t, s) = \frac{\varepsilon_{ijk} V_{0,i} \mathfrak{I}[\mathcal{W}_j^*(t, s)\mathcal{W}_k(t, s)]}{\pi} s, \quad (1)$$

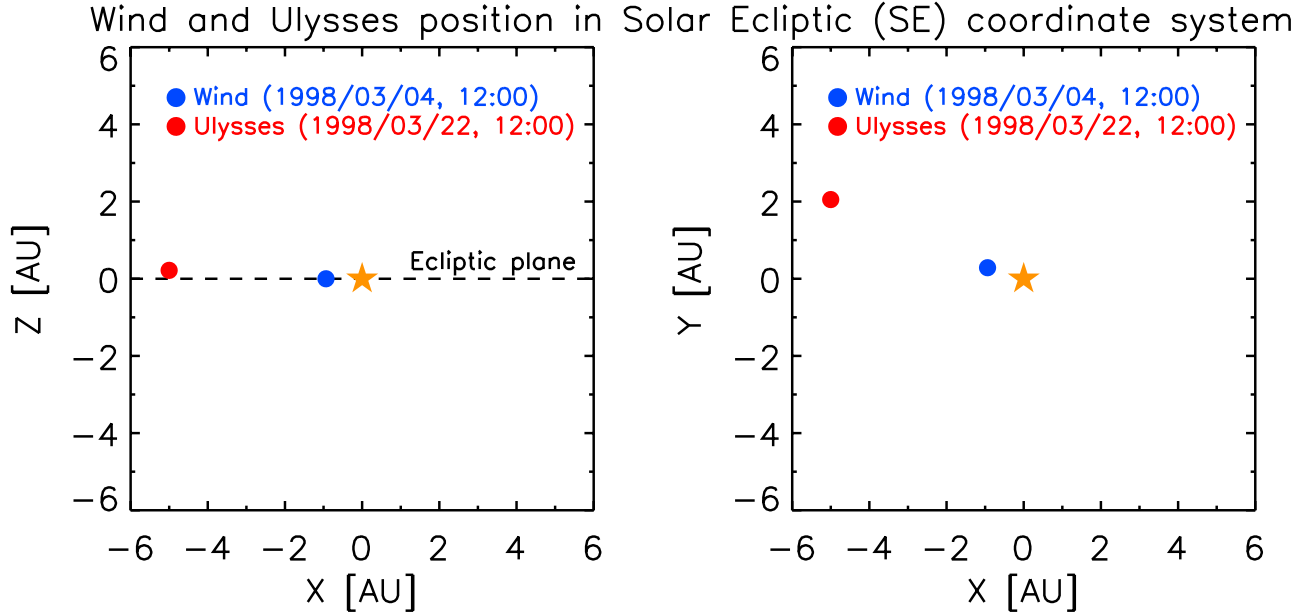$$H_c(t, s) = W^+(t, s) - W^-(t, s), \quad (2)$$

Figure 1. Wind (blue) and Ulysses (red) positions with respect to the Sun (yellow star), in side (left panel) and top (right panel) views of the ecliptic plane, at the times when the MC event of 1998 March was observed by them.

$$E_r(t, s) = W_u(t, s) - W_b(t, s), \tag{3}$$

$$E(t, s) = W_u(t, s) + W_b(t, s), \tag{4}$$

where ε_{ijk} is the antisymmetric Levi-Civita symbol; $*$ and $\mathfrak{I}$ denote, respectively, the complex conjugate and imaginary part; $\mathcal{W}_i$ ($i = 1, 2, 3$) is the wavelet transform of the i-component of the magnetic field; $W^\pm$ are the wavelet power spectra of the Elsässer variables, namely (in Einstein notation), $W^\pm = \mathcal{W}(z_i^\pm)\mathcal{W}^*(z^{\pm i})$; and W_u and W_b are the wavelet power spectra of the kinetic and magnetic energy, namely, $W_u = \mathcal{W}(u_i)\mathcal{W}^*(u^i)$ and $W_b = \mathcal{W}(b_i)\mathcal{W}^*(b^i)$. It transpires that a positive (negative) value of H_c indicates a net outward (inward) energy flux for Alfvénic fluctuations, while $H_c \sim 0$ indicates balance of the Alfvén mode fluxes. Likewise, $E_r \gtrless 0$ indicates kinetic or magnetic energy dominance, while $E_r \sim 0$ is indicative of energy equipartition. Less intuitively, from the sign of H_m it is possible to derive the handedness of the magnetic field: $H_m \gtrless 0$ corresponds to (counter)clockwise rotations of the magnetic field vector in the plane perpendicular to the sampling direction, namely, to (right) left-handed chirality, while $H_m \sim 0$ indicates untwisted magnetic field lines.

The normalized forms of Equations (1)–(3), $\sigma_m(t, s)$, $\sigma_c(t, s)$, and $\sigma_r(t, s)$, are

$$\sigma_m(t, s) = 2\frac{\varepsilon_{ijk}V_{0,i}\mathfrak{I}[\mathcal{W}_j^*(t, s)\mathcal{W}_k(t, s)]}{V_0\mathcal{W}_\mu^*\mathcal{W}^\mu}, \tag{5}$$

$$\sigma_c(t, s) = \frac{W^+(t, s) - W^-(t, s)}{W^+(t, s) + W^-(t, s)}, \tag{6}$$

$$\sigma_r(t, s) = \frac{W_u(t, s) - W_b(t, s)}{W_u(t, s) + W_b(t, s)}. \tag{7}$$

In the unperturbed solar wind, magnetic helicity, cross-helicity, residual, and total energy fluctuations drop off according to power laws (see also Matthaeus & Goldstein 1982; Bruno & Dobrowolny 1986), with spectral slopes depending on

the considered scale range. Thus, similar to Telloni et al. (2012, 2013, 2019), the corresponding scalograms derived from Equations (1)−(4) are compensated by dividing $H_m(t, s)$, $H_c(t, s)$, $E_r(t, s)$, and $E(t, s)$ by s^α, s^β, s^γ, and s^δ, respectively. The spectral indexes α, β, γ, and δ have been accurately inferred by fitting, with a power-law function in the scale range of interest, the spectral densities of H_m, H_c, E_r, and E, computed via a fast Fourier transform on the same data. This enhances helicity events immersed in the solar wind and potentially overshadowed by large-scale flux tubes roughly aligned to the local Parker's spiral (Matthaeus & Goldstein 1982) and reveals turbulent features at scales much smaller than characteristic of the main event, i.e., the MC.

3. Results

The wavelet analysis is applied to 8 and 23 day intervals centered around the arrival times of the MC at Wind and Ulysses, respectively. The corresponding results are shown in Figure 2. Left and right panels refer to Wind and Ulysses observations, respectively. Figures 2(a) (left and right) show in situ measurements from the instruments on board the two satellites; specifically, the time profiles of the components of the plasma velocity fluctuations δV_i and magnetic field B_i, and of the proton number density n_p, are displayed. Figures 2(b)–(e) show the scalograms, in the 4–128 (Wind) and 8–512 (Ulysses) hr scale ranges, of the magnetic helicity, cross-helicity, residual energy, and total energy, derived from Equations (1)−(4), and compensated as described above. The cross-hatched areas correspond to the cones of influence (COI), where edge effects, due to finite-length time series, may affect the reliability of the computed MHD parameters. The dashed vertical lines indicate the MC boundaries reported in Nakwacki et al. (2011).

The MC embedded in the ICME is clearly visible at both heliocentric distances as a large-scale, left-handed magnetic helical structure with a highly positive H_m (Figures 2(b)), more energetic than the surrounding solar wind plasma (Figures 2(e)). The dashed and thick lines in Figures 2(b) enclose regions where
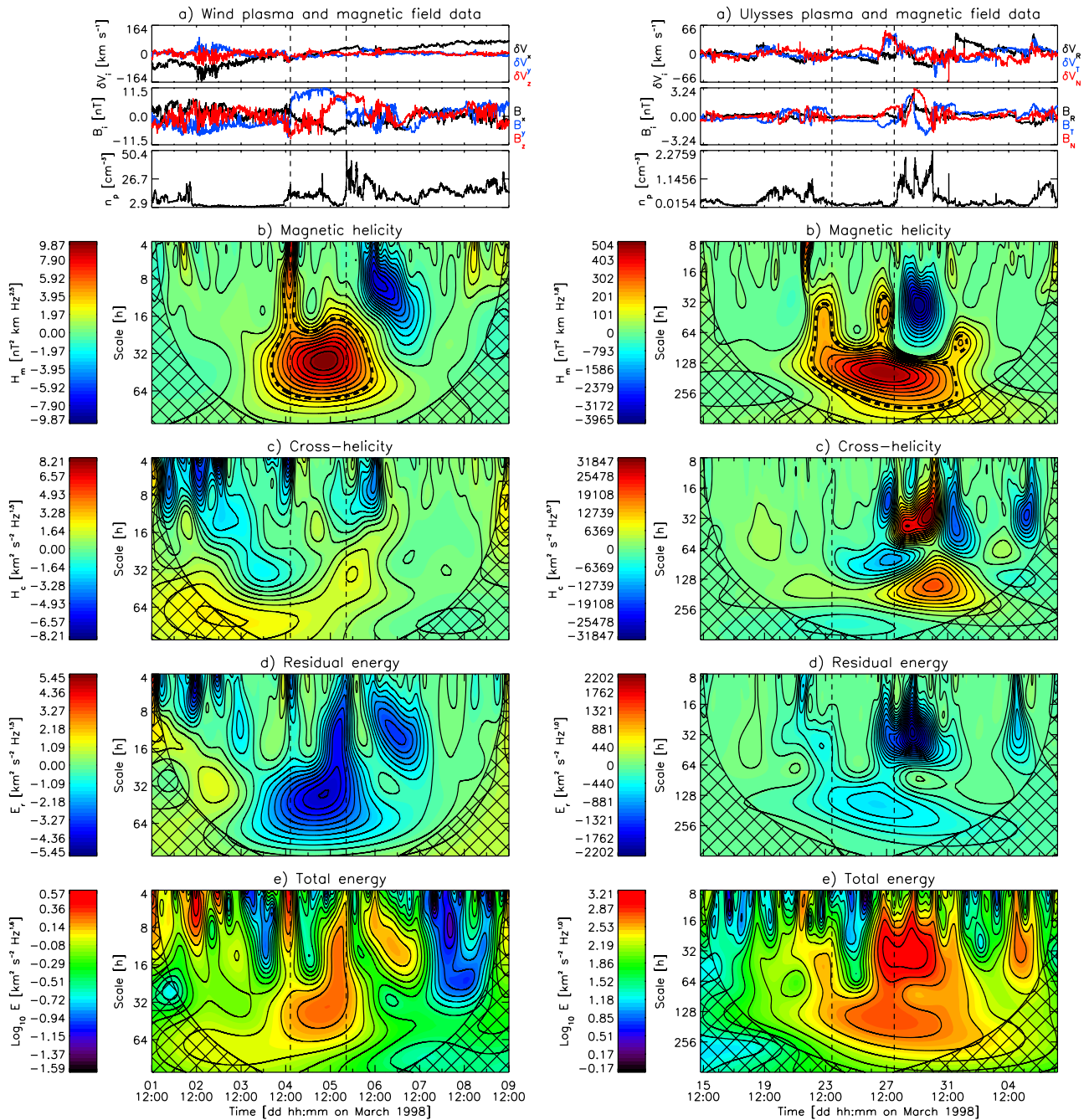
Figure 2. Overview of the MHD properties of the MC observed by Wind at 1 au (left panels) and Ulysses at 5.4 au (right panels). From top to bottom, the panels show the time series of the components of the plasma velocity fluctuations and magnetic field vector, and of the proton number density (a), and the compensated scalograms of H_m (b), H_c (c), E_r (d), and E (e). The cross-hatched areas in panels (b)−(e) mark the COI, where estimates of the MHD quantities are not considered fully reliable. The dashed and thick contours in panels (b) correspond to the $1/e$ value of the maximum magnetic helicity content within the MC. The event identified by Nakwacki et al. (2011) is delimited by dashed vertical lines.

H_m is larger than the $1/e$ value of the maximum within the MC. These are very useful to assess the temporal extension of the MC and the characteristic scale corresponding to the winding of the magnetic field lines around the MC axis. The MC is about 4.5 times longer at Ulysses than at Earth, increasing from 2.3 to 10.2 days. Hence, the MC expands during its transit from 1 to 5.4 au at a rate $\alpha = 0.89$, in agreement with expectations (MC radial size has indeed been observed statistically to increase with distance R from the Sun as R^α, with $\alpha \in (0.7, 1)$; Bothmer & Schwenn 1998; Liu et al. 2005). Accordingly, the characteristic scale increases from 38.1 to 152.2 hr ($\alpha = 0.89$). Some

discrepancies are however found with the MC boundaries inferred at 5.4 au from the velocity and magnetic field profiles by Nakwacki et al. (2011) (dashed vertical lines in Figure 2): although the MC core (identified by the highest magnetic helicity value) falls fairly well in the middle of the boundaries identified by Nakwacki et al. (2011), the magnetic helicity feature corresponding to the MC extends well beyond the previously reported back boundary. As a result, the MC extension computed in Nakwacki et al. (2011) was remarkably smaller (~4 days), as well as the expansion rate ($\alpha \simeq 0.7$), than that found in the present analysis.

A helical structure with opposite handedness ($H_m \ll 0$) is observed downstream of the MC at both 1 and 5.4 au, at scales around 8 and 35 hr, respectively (Figures 2(b)). A first glance might suggest that this corresponds to the same event observed at two different heliocentric distances by the two aligned spacecraft. However, a closer analysis of the corresponding sizes at Wind and Ulysses positions (1.2 and 2.1 days, respectively) suggests that these may not be consistent with the expected radial expansion R^α, in fact implying $\alpha = 0.33$. Moreover, a comparison of the characteristic scales leads to $\alpha = 0.87$, in contrast with the expectations that MC size and pitch of the magnetic field wrapping should scale similarly. Furthermore, the helical structure is more twisted at Ulysses than at Earth ($\sigma_m = -0.73$ and -0.82 at 1 and 5.4 au, respectively), and while a degradation of the MC field winding throughout the interplanetary space can be somehow anticipated (for instance, by means of magnetic erosion-related processes), it is more difficult to explain how an expanding solar event could become more strongly twisted during its evolution. On the other hand, a low value of α is not a sufficient reason to discard a solar origin and the consequent expansion of the observed structure. In fact, ICMEs with dispersed values of α, mainly due to the interaction with other solar wind structures (e.g., high-speed streams or another ICME as can be the case analyzed here), have been observed quite often (Gulisano et al. 2010, 2012). Hence, the reason the helical structure does not increase as much as expected could be due to interaction with the preceding MC via (as discussed below) magnetic reconnection-related processes, which could peel away the outer layer (Dasso et al. 2006), leaving a more twisted core. While this is not consistent with the Lundquist picture of an MC as a flux rope with a highly twisted outer layer and a less twisted core (Lanabere et al. 2020), it might be consistent with other models of an MC. In addition, Skoug et al. (2000) interpreted the structure observed at Earth as a non-MC ICME. It follows that two different scenarios are possible: the highly negative magnetic helicity signature displayed in the H_m scalograms at Wind and Ulysses may indeed correspond to either the same structure observed at two different stages of interaction with the preceding ICME, or to two different structures. Specifically, the fulfillment of the Walén test (not shown) in the corresponding interval at Wind position indicates that the structure observed at 1 au might rather be a flux rope generated locally via magnetic reconnection processes and then no longer observed at 5.4 au. Conversely, as also indicated by Skoug et al. (2000), the structure observed at Ulysses is likely a second MC of solar origin, which would have propagated faster that the preceding one, reaching and compressing it at 5.4 au (as evidenced by the enhancements in density/magnetic field profiles at the MC–MC interface, consistent with a compression region). In spite of the two possibilities, what clearly emerges from this analysis is that at 5.4 au the second MC is heavily interacting with the first one. As a result, the magnetic structure of the preceding MC is strongly deformed. In fact, its large-scale rotation extends well beyond the rear of the following MC and represents de facto a form of background magnetic field rotation. Rotations with opposite helicity, associated with the following MC, are superposed at smaller scales. This scenario is clearly evidenced by the H_m scalogram (right panel of Figure 2(b)).

The radial evolution exhibited by the MHD quantities within the left-handed MC from 1 to 5.4 au corresponds to a typical magnetic cloud, showing, as expected, close-to-zero cross-helicity (Figures 2(c), in accordance with recent findings by Good et al. 2020) and an excess of magnetic energy ($E_r < 0$; Figures 2(d)). However, while the averaged $|\sigma_c|$ over the MC region bounded by the dashed contour line in Figures 2(b) is constant with a value of 0.09 throughout the heliosphere, the dominance of the magnetic energy is reduced during propagation ($\sigma_r = -0.79$ and -0.62 at 1 and 5.4 au, respectively), from 93% to 82% of the total energy. It follows that the MC kinetic energy increases from 7% to 18%. Moreover, the normalized magnetic helicity is reduced (from $\sigma_m = 0.83$ to $\sigma_m = 0.67$ in moving from 1 to 5.4 au), indicating that the high degree of twisting of the MC field topology relaxes as it propagates outward. The background-comparable density inside the MC at 5.4 au (different than 1 au) might be due to the low helicity, which is not strong enough to maintain the density, resulting in leakage along the field lines. It appears that some mechanism is at work in converting magnetic energy into kinetic energy, making the MC less magnetically wound.

This process is likely ascribed to magnetic erosion by the following MC. The opposite helicity of the two MCs should mean that the magnetic field direction at the interface is the same, if the two MCs had the same orientation of the axial field. However, the Grad–Shafranov (GS; Hau & Sonnerup 1999; Hu & Sonnerup 2001) reconstruction of the two MCs reveals that they have quite different orientation axes (specifically the polar θ and azimuthal ϕ angles are $\theta = 70°$ and 40°, and $\phi = 260°$ and 20°),[9] implying that the magnetic field lines at their interface are opposite to some extent. In the interaction region, the opposed fields of the rear and front of the two successive MCs come into contact, thus magnetically reconnecting and causing the preceding MC to be heavily deformed. As a matter of fact, the MC helicity configuration is much more complex (and less confined in scale) at Ulysses than at Earth (Figures 2(b)), with tails of positive magnetic helicity remarkably protruding from the major helical structure at smaller scales both in the central and downstream region. The tail observed in the upstream region at both 1 and 5.4 au might be ascribed to enhanced magnetic field fluctuations located at the interaction border between the sheath and MC. The somewhat smoother shape exhibited at Ulysses is probably due to turbulent evolution during the MC propagation. These minor helical structures likely result from the magnetic erosion of the outer layer of the preceding MC by the following one. Any magnetic reconnection event is accompanied by a rearrangement of the magnetic field topology and conversion of magnetic energy into kinetic energy (among other forms of energy). In this scenario, the degradation of the helical configuration of the MC observed at 5.4 au along with a less imbalanced energy budget favoring an increase of kinetic energy fluctuations can be easily interpreted. The interaction is even stronger and the magnetic reconnection-related processes are even more efficient when the same characteristic scales are involved (reconnection processes between two flux-rope-like structures are more effective when the pitch of the magnetic field wrapping is the same). Hence, at scales around 32 hr, the interaction between the following MC with one of the tails of the preceding one protruding at smaller scales on 1998 March 27 (where $\sigma_m = 0.66$ and the magnetic energy is further less dominant, being 77% of the total) is so strong (the total energy

---

9   For the two MCs, see http://fluxrope.info/.

in the interaction region is larger than that inside the MC) that this tail is almost completely disconnected from the main event. Nakwacki et al. (2011) identified a shock here (1998 March 26 at 22:00 UT), after which they found that the MC is strongly distorted, consistent with the present results. Partial disconnection from the major structure is also observed at the trailing edge of the MC, where the tail elongation at smaller scales on 1998 April 1 is characterized by a quasi-energy balance state ($\sigma_r = -0.19$).

Regarding the radial evolution of the cross-helicity within the MC, it is worth noting that while at 1 au H_c is close to zero not only, as expected, in the MC core but also in the upstream and downstream regions, the cross-helicity configuration downstream of the MC as observed at 5.4 is much more complex. Both positive and negative features overlap at different scales, particularly in the MC–MC interaction region (Figure 2(c)). A possible reason for the cross-helicity changing is because of the coupling of the MC to the large-scale gradient flow, which might cause slab Alfvénic fluctuations to develop, thus increasing σ_c (Zank et al. 2017; Adhikari et al. 2020). Another or possibly related reason is that observations at 5.4 au may be attributed to the presence of Alfvénic fluctuations in the MC's outer layer (as also found by Good et al. 2020), which may have been locally generated by the interaction of the MC and the surrounding solar wind. As the MC evolves, its outer layers are gradually eroded by small-scale reconnection with the background magnetic field through which it propagates, and that will give rise to oppositely directed Alfvén waves as a potential signature. Furthermore, at the interaction region where the two MC outer layers come into contact, sunward and antisunward Alfvénic fluctuations at different scales may mix together, driving the more complex cross-helicity scenario depicted in the σ_c scalogram (right panel of Figure 2(c)).

Finally, regarding the $H_m < 0$ structure observed at 1 au (left panel of Figure 2(b)), it might be interpreted, as discussed above, as a flux rope of local origin that is no longer observed at 5.4 au. A possible reason is that its lifetime is less than the propagation time from the Wind to Ulysses locations. Since the flux rope can be viewed as representative of quasi-2D turbulence, its lifetime can be estimated by the turbulence nonlinear time $\tau_{nl} \simeq \ell \langle \delta z^2 \rangle^{-1/2}$, where ℓ is the characteristic scale of the flux rope (related to the characteristic timescale τ under Taylor's hypothesis, $\ell \sim \tau \cdot V_0$) and $\langle \delta z^2 \rangle^{1/2}$ is the standard deviation of the fluctuating Elsässer variables. Using $\ell \sim 0.07$ au ($\tau \sim 8$ hr and $V_0 \sim 340$ km s^{-1}) and $\langle \delta z^2 \rangle^{1/2} \sim 15$ km s^{-1}, the nonlinear time is about $\tau_{nl} \simeq 6.5 \times 10^5$ s. Assuming a constant solar wind speed of $V_0 \sim 340$ km s^{-1}, the propagation time from 1 to 5.4 au is about 1.9×10^6 s, which is 3 times longer than the expected lifetime of the flux rope. In other words, the flux rope might have turbulently decayed by the time it should have reached the Ulysses spacecraft. An alternative explanation might be that the in situ generated flux rope merged with the following MC (which has the same handedness) through a coalescence process (Zhao et al. 2019).

4. Conclusions

The investigation of the radial evolution of the MHD characteristics of an MC observed at 1 au by Wind and at 5.4 au by Ulysses yielded surprising results about the turbulent evolution of the ICME during its propagation from Earth into the outer heliosphere. This analysis provides the first direct 2D visualization of magnetic erosion between two interacting MCs. Interfaces between adjacent flux tubes are of great interest since they are where fundamental plasma physical processes, such as turbulence and magnetic reconnection, occur. Due to the underlying magnetic reconnection occurring at the MC–MC interface, the leading MC field is heavily deformed, thus experiencing significant restructuring and weakening of the highly wrapped magnetic field configuration exhibited at 1 au, with consequent implications for the conservation of magnetic helicity with distance from the Sun.

This novel study can stimulate similar analyses carried out using radial alignments of recently launched planetary and solar missions, such as BepiColombo, Solar Orbiter, and Parker Solar Probe (which will orbit the Sun at very different distances). Recognized by many scientists as the golden age of the physics of the Sun and planetary systems, this unprecedented observational capability will allow in-depth investigation of MHD turbulent evolution of CMEs from the solar corona into interplanetary space.

ORCID iDs

Daniele Telloni ⓘ https://orcid.org/0000-0002-6710-8142
Lingling Zhao ⓘ https://orcid.org/0000-0002-4299-0490
Gary P. Zank ⓘ https://orcid.org/0000-0002-4642-6192
Haoming Liang ⓘ https://orcid.org/0000-0001-9581-4821
Masaru Nakanotani ⓘ https://orcid.org/0000-0002-7203-0730
Laxman Adhikari ⓘ https://orcid.org/0000-0003-1549-5256
Francesco Carbone ⓘ https://orcid.org/0000-0002-3559-5273
Raffaella D'Amicis ⓘ https://orcid.org/0000-0003-2647-117X
Denise Perrone ⓘ https://orcid.org/0000-0003-1059-4853
Roberto Bruno ⓘ https://orcid.org/0000-0002-2152-0115
Sergio Dasso ⓘ https://orcid.org/0000-0002-7680-4721

References

Adhikari, L., Zank, G. P., & Zhao, L.-L. 2020, ApJ, 901, 102
Al-Haddad, N., Roussev, I. I., Möstl, C., et al. 2011, ApJL, 738, L18
Balogh, A., Beek, T. J., Forsyth, R. J., et al. 1992, A&AS, 92, 221
Bame, S. J., McComas, D. J., Barraclough, B. L., et al. 1992, A&AS, 92, 237
Bothmer, V, & Schwenn, R. , 1998, AnGeo, 16, 1
Bruno, R., & Carbone, V. 2013, LRSP, 10, 2
Bruno, R., & Dobrowolny, M. 1986, AnGeo, 4, 17
Burlaga, L. F. 1988, JGR, 93, 7217
Burlaga, L. F., Sittler, E., Mariani, F., & Schwenn, R. 1981, JGR, 86, 6673
Dasso, S., Mandrini, C. H., Démoulin, P., & Luoni, M. L. 2006, A&A, 455, 349
Du, D., Wang, C., & Hu, Q. 2007, JGR, 112, A09101
Elsässer, W. M. 1950, PhRvL, 79, 183
Good, S. W., Kilpua, E. K. J., Ala-Lahti, M., et al. 2020, ApJL, 900, L32
Gulisano, A. M., Démoulin, P., Dasso, S., & Rodriguez, L. 2012, A&A, 543, A107
Gulisano, A. M., Démoulin, P., Dasso, S., Ruiz, M. E., & Marsch, E. 2010, A&A, 509, A39
Hau, L.-N., & Sonnerup, B. U. Ö 1999, JGR, 104, 6899

Hu, Q., & Sonnerup, B. U. Ö 2001, GeoRL, 28, 467
Kilpua, E. K. J., Koskinen, H. E. J., & Pulkkinen, T. I. 2017, LRSP, 14, 5
Klein, L. W., & Burlaga, L. F. 1982, JGR, 87, 613
Lanabere, V., Dasso, S., Démoulin, P., et al. 2020, A&A, 635, A85
Lepping, R. P., Acũna, M. H., Burlaga, L. F., et al. 1995, SSRv, 71, 207
Lepping, R. P., Jones, J. A., & Burlaga, L. F. 1990, JGR, 95, 11957
Li, H., Wang, C., Richardson, J. D., & Tu, C. 2017, ApJL, 851, L2
Liu, Y., Richardson, J. D., & Belcher, J. W. 2005, P&SS, 53, 3
Lugaz, N., Salman, T. M., Winslow, R. M., et al. 2020, ApJL, 899, 119L
Manchester, W., Kilpua, E. K. J., Liu, Y. D., et al. 2017, SSRv, 212, 1159
Matthaeus, W. H., & Goldstein, M. L. 1982, JGR, 87, 6011
Moffatt, H. K. 1978, Magnetic Field Generation in Electrically Conducting Fluids (Cambridge: Cambridge Univ. Press)
Nakwacki, M. S., Dasso, S., Démoulin, P., Mandrini, C. H., & Gulisano, A. M. 2011, A&A, 535, A52
Ogilvie, K., Chornay, D., Fritzenreiter, R., et al. 1995, SSRv, 71, 55

Reames, D. V. 1999, SSRv, 90, 413
Richardson, I. G., & Cane, H. V. 2010, SoPh, 264, 189
Russell, C. T., & Elphic, R. C. 1979, Natur, 279, 616
Salman, T. M., Winslow, R. M., & Lugaz, N. 2020, JGR, 125, e27084
Skoug, R. M., Feldman, W. C., Gosling, J. T., et al. 2000, JGR, 105, 27269
Telloni, D., Antonucci, E., Bemporad, A., et al. 2019, ApJ, 885, 120
Telloni, D., Bruno, R., D'Amicis, R., et al. 2012, ApJ, 751, 19
Telloni, D., Carbone, V., Perri, S., et al. 2016, ApJ, 826, 205
Telloni, D., Perri, S., Bruno, R., et al. 2013, ApJ, 776, 3
Torrence, C., & Compo, G. P. 1998, BAMS, 79, 61
Vourlidas, A. 2014, PPCF, 56, 064001
Zank, G. P., Adhikari, L., Hunana, P., et al. 2017, ApJ, 835, 147
Zhao, L.-L., Zank, G. P., Adhikari, L., et al. 2020a, ApJS, 246, 26
Zhao, L.-L., Zank, G. P., Hu, Q., et al. 2020b, A&A, in press
Zhao, Y., Feng, H., Liu, Q., & Zhao, G. 2019, FrP, 7, 151